🔓 OPEN ACCESS

The focal adhesion protein talin is a mechanically gated A-kinase anchoring protein

Mingu Kang[a,b,c,1] (ID), Yasumi Otani[d,e,1] (ID), Yanyu Guo[f] (ID), Jie Yan[f] (ID), Benjamin T. Goult[d,e,2] (ID), and Alan K. Howe[a,b,c,2] (ID)

Protein kinase A (PKA) is a ubiquitous, promiscuous kinase whose activity is specified through subcellular localization mediated by A-kinase anchoring proteins (AKAPs). PKA has complex roles as both an effector and a regulator of integrin-mediated cell adhesion to extracellular matrix (ECM). Recent observations demonstrate that PKA is an active component of focal adhesions (FA), suggesting the existence of one or more FA AKAPs. Using a promiscuous biotin ligase fused to PKA type-IIα regulatory (RIIα) subunits and subcellular fractionation, we identify the archetypal FA protein talin1 as an AKAP. Talin is a large, mechanosensitive scaffold that directly links integrins to actin filaments and promotes FA assembly by recruiting additional components in a force-dependent manner. The rod region of talin1 consists of 62 α-helices bundled into 13 rod domains, R1 to R13. Direct binding assays and NMR spectroscopy identify helix41 in the R9 subdomain of talin as the PKA binding site. PKA binding to helix41 requires unfolding of the R9 domain, which requires the linker region between R9 and R10. Experiments with single molecules and in cells manipulated to alter actomyosin contractility demonstrate that the PKA–talin interaction is regulated by mechanical force across the talin molecule. Finally, talin mutations that disrupt PKA binding also decrease levels of total and phosphorylated PKA RII subunits as well as phosphorylation of VASP, a known PKA substrate, within FA. These observations identify a mechanically gated anchoring protein for PKA, a force-dependent binding partner for talin1, and a potential pathway for adhesion-associated mechanotransduction.

mechanotransduction | talin | protein kinase A | signaling | cell adhesion

The cAMP-dependent protein kinase (protein kinase A; PKA) is the major receptor for the second messenger cAMP and is responsible for regulating myriad physiological and cellular processes. PKA is a heterotetrameric enzyme consisting of a dimer of regulatory (R) subunits that binds and sequesters two catalytic (C) subunits until cAMP binding to the R subunits causes C subunit release and activation (1). PKA is ubiquitous, with hundreds of substrates associated with numerous distinct signaling pathways and cellular functions throughout the cell (2), leading to an abiding challenge and effort to understand how specificity in PKA signaling is achieved.

A significant literature establishes that, despite its ubiquity, PKA and its activity are highly localized within cells (3–5). While PKA C subunits were classically thought to freely diffuse from cAMP-bound R subunits (1), recent impactful work supports a more restrained radius of activity through either maintenance of an intact, catalytically active tetrameric holoenzyme (6, 7) or restricted release and recapture of the C subunit (8, 9). Importantly, PKA activity is also localized through interaction (predominantly of type-II R subunits) with A-kinase anchoring proteins (AKAPs) that physically and functionally assign PKA to discrete subcellular niches (4, 10). AKAPs comprise a large, growing, and functionally diverse family of proteins with two common structural features: an amphipathic α-helix that mediates binding to R subunit dimers with nanomolar affinity and a complement of unique domains that specify distinct subcellular localization. In addition to anchoring PKA, AKAPs often scaffold substrates and regulators of PKA as well as other signaling proteins (4, 10). Thus, AKAPs mediate assembly and localization of discrete subcellular signaling nodes for PKA and allow this single kinase to participate in multiple, spatiotemporally distinct cellular processes.

Importantly, AKAP-mediated localization of PKA activity has been shown to regulate various aspects of cell migration (11–13). For example, PKA activity is enriched in the leading edge in a manner that requires both anchoring and actomyosin contractility (14–16). PKA has also been shown to be both a complex regulator and effector of integrin-mediated adhesion to the extracellular matrix (ECM) (11, 17–23), although the underlying molecular mechanisms are not fully understood. Recently (24), we reported

Significance

There is increasing interest in the ability of proteins involved in cell adhesion to convert mechanical force into altered biochemistry. Cellular signal transduction is most often conducted through multiprotein scaffolds that consolidate, localize, and specify signaling inputs and outputs. This report bridges these fields by identifying an interaction between talin, a mechanosensitive adhesion protein, and PKA, a pleiotropic kinase with myriad cellular targets. Together, these observations form the foundation for a mechanotransduction pathway that utilizes force-dependent changes in protein conformation to establish a solid-state signaling complex well positioned to couple cellular tension to cellular communication.

the presence of PKA subunits, activity, and novel substrates within focal adhesions (FAs), dynamic, multiprotein junctions formed between the cytoplasmic tails of ECM-bound integrins and actin microfilaments (25). This positioning means that FAs are subject to actomyosin-generated mechanical forces that alter the conformation of various FA components and thus regulate FA composition and dynamics (26–28). In addition to their structural role, FAs are solid-state signaling centers that scaffold kinases, phosphatases, and other enzymes to transmit and control the state of integrin-mediated cell adhesion and mechanosensing (26–29). Central to this mechanosensitive machinery is the protein talin, which directly couples integrins to F-actin (30, 31). The C terminus of talin is an extended rod comprised of 62 α-helices arranged in 13 modular bundles, R1 to R13, that serve as force-dependent switch domains by opening and closing in response to small changes in contractility, thereby recruiting and displacing a myriad of interacting proteins enabling talin to serve as a mechanosensitive signaling hub (31). While many proteins have been identified that bind to the folded switch domains, only vinculin has been reported to bind to the unfolded domains, as its binding requires exposure of cryptic vinculin binding sites, comprising single amphipathic helices where the epitope is buried within the folded rod domain (32–34).

The functional connections between PKA and cell adhesion (11, 13), the presence of PKA subunits and activity within FAs (24), and the precept that AKAPs establish and colocalize with PKA activity microdomains (35) led us to search for potential AKAPs within FAs. In this study, we identify that PKA binds directly to an α-helix in talin that is cryptic and exposed only when the R9 domain unfolds, establishing talin as a mechanically gated AKAP and PKA as a mechanically gated signaling partner for talin.

Results

Identification of PKA RIIα-Binding Proteins in FA. As a preliminary test for the presence of AKAPs in FA, whole-cell extracts (WCE) and isolated focal adhesion cytoskeletal (FACS) fractions were analyzed using an RII overlay assay (36), a blotting method in which a purified recombinant V5 epitope-tagged docking/dimerization domain of PKA RIIα (RIIα-D/D) is used in place of a primary antibody, allowing detection of AKAP–RIIα interactions using anti-V5 secondary antibody. Both whole cell extracts and isolated FACS fractions exhibited broad RIIα-binding activity over a wide range of molecular weights (*SI Appendix*, Fig. S1) that was significantly diminished by Ht31, an AKAP-derived peptide that binds to PKA R subunit D/D domains and thus competitively inhibits PKA–AKAP interactions (36), but not by the inactive control peptide Ht31p. These observations indicate the presence of AKAPs in FACS fractions.

To identify potential FA AKAPs, we used proximity-dependent biotinylation catalyzed by a V5 epitope-tagged miniTurbo (mTb) biotin ligase (37) attached to the C terminus of PKA RIIα. The mTb ligase biotinylates proteins in a ~35 nm radius (37), so we hypothesized that RIIα-mTb would biotinylate AKAPs and proximal AKAP-associated proteins (Fig. 1*A*). Expression of V5-RIIα-mTb resulted in robust protein biotinylation in a manner dependent on exogenous biotin (*SI Appendix*, Fig. S2A) and with a pattern quite distinct from that catalyzed by ER-mTb, a well-characterized mTb targeted to the ER membrane (37). To increase experimental control of biotin labeling, we generated a stable line of U2OS cells in which the expression of V5-RIIα-mTb and consequent biotinylation are controlled by a doxycycline-inducible promoter (Fig. 1 *B* and *C*). Importantly, induced expression of V5-RIIα-mTb did not suppress bulk PKA activity (*SI Appendix*, Fig. S2B). Moreover, V5-RIIα-mTb, like endogenous RIIα subunits (24), was present in isolated FACS fractions (Fig. 1*D*) and catalyzed biotinylation of FACS proteins (Fig. 1*E*). Thus, FACS fractions from RIIα-mTb-expressing cells (or uninduced control cells) were collected and biotinylated proteins were isolated using streptavidin beads then characterized by LC–MS/MS-based proteomics (Fig. 1*F*). A total of 326 proteins were present either exclusively or at least fivefold higher in doxycycline-induced *vs* uninduced samples (Fig. 1*G* and Dataset S1). This list was narrowed as shown in Fig. 1*G*. Briefly, we excluded proteins not present in the "meta-adhesome" [a compilation of FA proteomic datasets (28, 38–41)], leaving 230 hits, and further refined this list by selecting proteins in the more exclusive "consensus core adhesome" (28), comprising proteins common to all published FA proteomes. This list of 18 hits was then compared to a list of in silico predicted
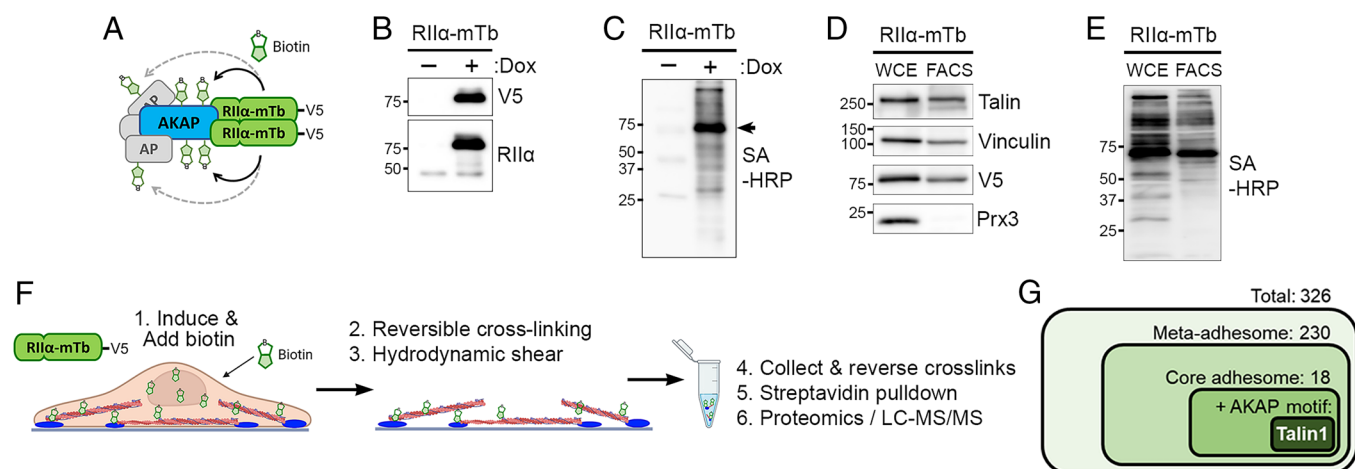

Fig. 1. Proximity-dependent biotin labeling reveals potential focal adhesion AKAPs. (*A*) Schematic of the approach, using the miniTurbo (mTb) biotin ligase fused to PKA RIIα to biotinylate AKAPs and associated proteins (*AP*). (*B* and *C*) U2OS cells stably expressing V5-tagged PKA RIIα-mTb under a doxycycline-inducible promoter were induced (+*Dox*) and labeled with biotin. Lysates were analyzed by blotting with the indicated antibodies (*B*) or streptavidin-conjugated HRP (SA-HRP; *C*). (*D* and *E*) Whole cell extracts (WCE) or focal adhesion/cytoskeleton (FACS) fractions made from Dox-induced cells were immunoblotted with the indicated antibodies (*D*) or SA-HRP (*E*). (*F*) Schematic of the FA AKAP screening protocol. (*G*) Bioinformatic pipeline for vetting candidate FA AKAPs. Hits from proteomic analysis were initially screened for inclusion in a combined "meta-adhesome" then for inclusion in the consensus core adhesome, and for the presence of a high-scoring, in silico–predicted potential AKAP motif. The only surviving hit was talin1.

AKAPs (42) generated by algorithmic scanning and scoring of protein sequences for homology to the degenerate PKA RIIα binding motif (*SI Appendix*, Fig. S5). For this stringent comparison, only proteins with a MAST [Motif Alignment and Search Tool, MEME Suite) score ≤50 (a cutoff that retains >95% of known AKAPs (42)] were considered. The only proteins surviving this vetting were talin1 and talin2, two isoforms of the key regulator of integrin-cytoskeletal coupling (31). Given that the number of talin1 peptides identified by LC–MS/MS greatly outnumbered that of talin2 (337 vs. 2; Dataset S1), we chose talin1 for initial investigation.

Talin1 Is an AKAP. Talin1 is a crucial FA component, binding and activating integrins and coupling them directly to cytoskeletal actin (30, 31). Talin1 also contributes to integrin-mediated adhesion through interaction with myriad FA and signaling proteins that regulate FA assembly, adhesive signaling, and mechanosensing (30, 31). To determine whether talin1 is indeed an AKAP, we directly assessed talin-PKA interaction. Talin immunoprecipitated from biotin-labeled, V5-RIIα-mTb-expressing cells is detectable by streptavidin-HRP (Fig. 2*A*), confirming that talin is directly biotinylated by RIIα-mTb and not present in the dataset due to indirect interaction with a biotinylated intermediate. Expression of an RIIα-mTb with point-mutations (I3S, I5S) known to disrupt RII-AKAP interactions (43, 44) significantly reduced the amount of both AKAP79 [a well-characterized AKAP (45)] and talin in streptavidin pull-downs compared to WT RIIα-mTb levels (Fig. 2*B*). Furthermore, both AKAP79 and talin coimmunoprecipitated with PKA RIIα-mTb under cross-linking conditions (Fig. 2*C*). These results support a close molecular interaction between talin and PKA RIIα but do not directly demonstrate that the interaction is direct—a sine qua non requirement for classification as an AKAP.

Talin1 is a large (~270 kDa) protein comprising an N-terminal globular head domain connected to an extensible rod domain comprising 62 helices arranged in 13 helical bundle domains (R1 to R13) with a helical dimerization domain (DD) at the C terminus (30, 46). In silico AKAP prediction software identified four of these 62 amphipathic helices (Fig. 2*D*) as putative PKA RIIα binding sites (42). To test whether talin interacts directly with PKA RIIα, constructs that divide the rod into four fragments—R1-3, R4-8, R9-12, and R13-DD, each containing one of the four in silico–predicted RIIα binding sites (Fig. 2*D*)—were used for recombinant protein expression (47) and purified fragments were analyzed by PKA RIIα overlay assay. Importantly, the denaturation and in situ refolding steps in this assay promotes refolding of individual α-helices but not of higher-order tertiary structures such as helical bundles (48–50). Strikingly, only the fragment comprising talin1 rod domains R9-12 bound directly to both the PKA RIIα D/D domain (Fig. 2*E*) and to purified, full-length PKA RIIα (*SI Appendix*, Fig. S3). This interaction could be specifically inhibited by the Ht31 inhibitor peptide indicating a canonical AKAP interaction. Furthermore, the interaction of talin1 R9-12 with PKA RIIα was comparable to that of the known AKAP, ezrin (Fig. 2*F*), a membrane-associated cytoskeletal linker (51). Taken together, these data indicate that talin1 directly binds PKA RIIα and establishes talin1 as a potential AKAP.

The R9 and R10 Domains of Talin1 Are Required, but Neither Is Sufficient, for PKA RIIα Binding. The in silico–predicted PKA RIIα binding motif within the R9-R12 fragment is helix 50 (h50) in the R11 domain (*SI Appendix*, Fig. S4), which shows significant homology to the canonical amphipathic helical motif for AKAPs (*SI Appendix*, Fig. S5). To determine whether talin h50 mediates binding to PKA, we mutated a key residue on the hydrophobic face of the helix, V2087, which would be predicted to abolish interaction with PKA RIIα (36). Specifically, we generated three

mutant talin1 R9-12 fragments targeting V2087—V2087P introduces a helix-breaking proline [analogous to the proline in the inactive Ht31p control peptide (36)], while V2087S interrupts the hydrophobic surface of h50 and the conservative V2087A replaces valine with the smallest hydrophobic residue alanine. Surprisingly, all mutant fragments, including V2087P, bound PKA RIIα D/D in overlay assays (*SI Appendix*, Fig. S4), strongly suggesting that h50, despite predictions and homology, is not the PKA RII binding site in talin.

We reverted to an empirical approach to map the binding site, performing overlay assays with serial truncations of the RIIα-binding R9-12 fragment (Fig. 3*A*). Removal of R12 and R11 did not disrupt talin-RIIα interaction, confirming that h50 is not the PKA binding site. Furthermore, while R9-10 still bound RIIα D/D, an isolated R9 domain did not (Fig. 3*A*), suggesting that R10 is essential for PKA RIIα binding. To confirm this, we performed additional overlay assays with R9-12 (ΔR10) and R10 alone (Fig. 3*B*). As expected, R9-12 (ΔR10) did not bind PKA RIIα D/D, reinforcing the hypothesized requirement for R10. Surprisingly, however, the R10 domain showed only very weak RIIα binding on its own (Fig. 3*B*). Together, these data indicate that the R9-10 domains are required for efficient binding to PKA and that neither R9 nor R10 alone is sufficient.

NMR Spectroscopy Reveals That Talin R9 Contains the RIIα Binding Site. The challenge of interpreting these RII overlay results prompted us to adopt a different methodology to assess the structural basis of the talin-PKA interaction. Thus, we used protein NMR spectroscopy—specifically, ^{1}H,^{15}N TROSY-HSQC experiments. HSQC spectra provide a powerful way to evaluate the structure of a protein, as each backbone amide gives rise to a discrete peak. When an unlabeled binding partner is added, changes to the spectral peaks can be detected. As reported previously, the NMR spectrum of talin1 R9-R10 shows good peak dispersion (46), and the spectra of the individual R9 and R10 domains overlay well indicating only limited interaction between the two domains [Fig. 3*C* and (46)]. Addition of unlabeled PKA RIIα D/D to ^{15}N-labeled R9-10 talin fragment confirmed a direct interaction of PKA to talin1 R9-10, as evidenced by significant changes in the talin spectra (Fig. 3*C*). A similar experiment with talin2 R9-R10 demonstrated that both talins can bind PKA (*SI Appendix*, Fig. S6). The nature of the spectral changes upon talin-PKA interaction was unexpected, however, as it showed a dramatic loss of a subset of the signals predominantly from the talin R9 domain, with the signals from the R10 domain largely unaffected (Fig. 3*C* and *SI Appendix*, Fig. S7). Specifically, addition of PKA RIIα D/D to talin R9-10 caused the signals from R9 to broaden and decrease in intensity (Fig. 3*C* and *SI Appendix*, Fig. S7A). This suggests that RIIα binding to R9-10 causes R9 to unfold and adopt a molten globule-like state, with broadened peaks indicative of an unfolded bundle but lacking the strong signal intensity of a fully extended polypeptide. In contrast, PKA RIIα D/D had minimal effect on the NMR spectra of individual R9 or R10 fragments, with only very small chemical shift changes in R9, indicative of a very weak interaction but no alteration in structure (Fig. 3*D*) and consistent with the inability of individual R9 or R10 to bind PKA in overlay assays (Fig. 3*B*). These NMR analyses indicate that the PKA RIIα D/D binds to R9-R10 primarily on R9, and is able to unfold the R9 domain but, intriguingly, only when attached to R10.

Helix41 in Talin R9 Domain Is the PKA RIIα Binding Site, but It Requires the R9-R10 Linker and Part of Helix42 from R10. AKAPs canonically use the hydrophobic face of an amphipathic helix to bind the RII dimer, and talin helices are arranged in bundles with the hydrophobic surfaces toward the center. Thus, we hypothesized
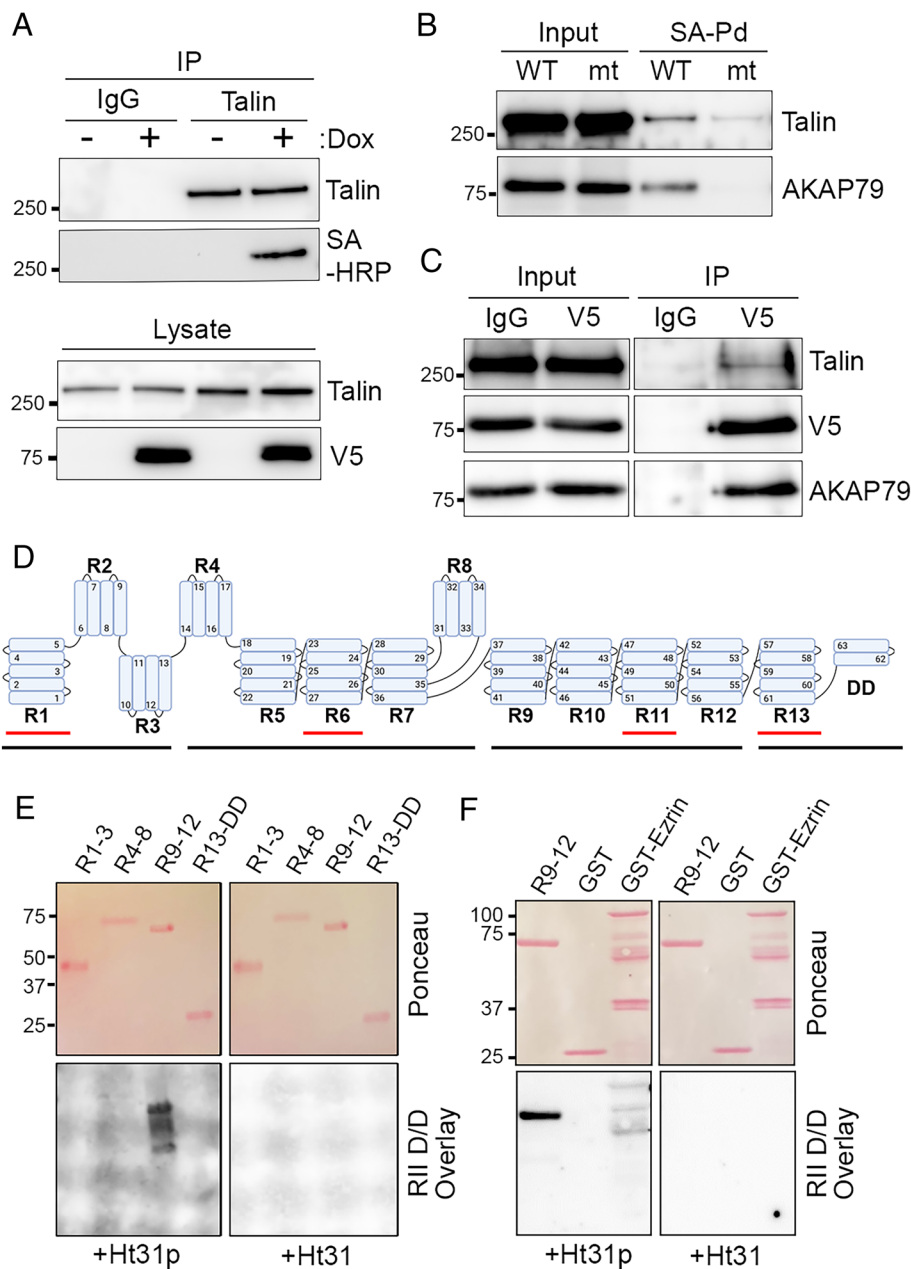
Fig. 2. Talin is an AKAP. (*A*) Cells were induced to express V5-RIIα-mTb and labeled with biotin. Lysates were directly blotted for talin or V5-RIIα-mTb or were immunoprecipitated with IgG or anti-talin antibody and then blotted with anti-talin antibody or streptavidin-HRP. Results are representative of seven independent immunoprecipitations. (*B*) Cells induced to express wild-type (WT) RIIα-mTb or a point-mutant deficient for AKAP binding (*mt*) were labeled with biotin. Lysates (Input) or streptavidin pull-downs (SA-Pd) were analyzed by immunoblotting for talin or AKAP79. (*C*) Lysates and control (IgG) or anti-V5 immunoprecipitates of DTBP-crosslinked, V5-RIIα-mTb-expressing cells were analyzed by immunoblotting. Results are representative of three independent immunoprecipitations. (*D*) Schematic of the talin1 rod, indicating the 13 rod (R) domains, R1-13, and the four fragments (black underline) used below. Each fragment contains an in silico–predicted RII-binding domain (red underline). (*E*) The fragments indicated in (*D*) were expressed recombinantly, separated by SDS-PAGE and transferred to membranes which were analyzed for equal loading (Ponceau) and then for direct PKA interaction by overlay with V5-tagged RIIα-dimerization/docking (RII D/D) domain in the presence of either a competitive blocking peptide (Ht31) or a nonblocking control (Ht31p). Results are representative of >5 similar overlays, with binding of R9-12 observed in >25 independent overlays. (*F*) Talin1 R9-12 fragment, GST alone, and GST-tagged ezrin were analyzed by RIIα D/D overlay as described in (*E*). Results are representative of eight independent overlays.

that the observed R9 unfolding is due to the RII-binding motif being on residues that are buried within the folded R9 5-helix bundle such that high-affinity PKA binding requires unfolding of the talin R9 domain to expose this motif. The paradigm of talin helix bundles unfolding in order to bind ligands is exemplified via the well-studied interaction between vinculin and the 11 talin helices that are vinculin-binding sites (VBS) (30, 31). To date, however, vinculin is the only protein identified that binds to open talin bundles. Furthermore, vinculin binding does not require

an adjacent domain being present to bind, unlike the currently observed requirements for PKA binding. Therefore, we next set out to identify how R10 was contributing to R9 unfolding and binding to PKA RII D/D. When we first resolved the domain boundaries of R10, we generated a series of constructs of R10 (52), including one 6-helix fragment—helix41-R10—comprising the last helix of R9 and the five helices of R10 (helices 41 to 46), so we tested whether this fragment was sufficient to bind PKA RIIα subunits. In the spectra of h41-R10, the signals corresponding
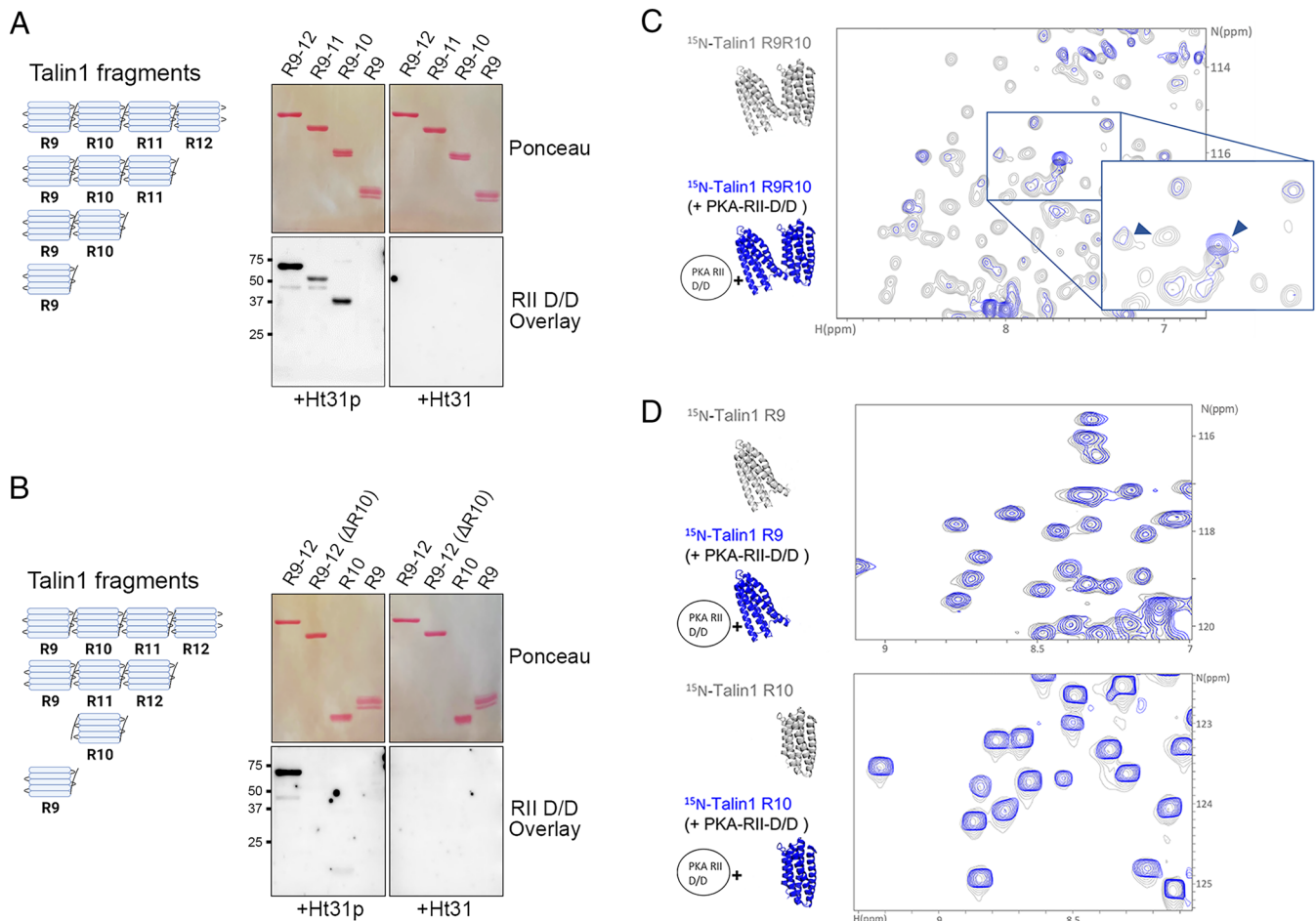
Fig. 3. The R9 and R10 domains of talin1 are required, but neither is sufficient, for PKA RIIα D/D binding. (*A* and *B*) Recombinant talin R9-12 and various R-subdomain truncation, deletion, or isolation fragments (*Left*) were analyzed by RIIα D/D overlay (*Right*) in the presence of either control Ht31p or AKAP-blocking Ht31 inhibitor peptides. Similar patterns of fragment binding were observed 9 (R9-10), 5 (R10), 4 (R9), and 2 (R9-12Δ10) overlays in various combined experiments. (*C*) ^{1}H,^{15}N HSQC spectra of ^{15}N-labeled talin R9-10 domains in the absence (gray) or presence (blue) of PKA RIIα D/D at a ratio of 1:5. Arrows indicate spectral peaks that disappear or shift in the presence of RIIα D/D. (*D*) ^{1}H,^{15}N HSQC spectra of individual ^{15}N-labeled talin R9 (*Top*) or R10 (*Bottom*) domains in the absence (gray) or presence (blue) of PKA RIIα D/D at a ratio of 1:3.

to h41 are readily identifiable by overlaying the spectra of R10 alone [*SI Appendix,* Fig. S8 and (52)]. As h41 is unbundled in this construct, it is unstructured, has only helical propensity and, as a result, its NMR peaks form a cluster of sharp signals with poor dispersion [*SI Appendix,* Fig. S8 and (52)], making it particularly amenable for visualizing shifts upon protein–protein interactions. Thus, ^{15}N-labeled talin1 h41-R10 fragment was analyzed by NMR in the absence and presence of PKA RIIα D/D (Fig. 4*A*). Upon addition of PKA RIIα D/D, chemical shift changes were visible, indicating binding of PKA to h41-R10. Moreover, the shifts were predominantly in the intense peaks that correspond to unbundled h41, with the signals both shifting and becoming less sharp as the helical conformation is stabilized upon binding (Fig. 4*A*).

Alignment of the h41 sequence with the PKA RII-binding motifs of known AKAPs shows significant similarities (*SI Appendix,* Fig. S5), most notably the semiregular spacing of aliphatic residues that form the requisite hydrophobic face on the helix. This alignment also reveals some significant deviations, most notably a pair of methionine residues in a position typically occupied by smaller aliphatics [Fig. 4*B* and *SI Appendix,* Fig. S5 (4, 36, 43)]—a deviation often associated with decreased affinity for RII subunits (36, 53) and likely responsible for the absence of h41 from in silico–predicted talin1 AKAP motifs (42). Given these considerations, along with the unique requirement of unfolding of R9 to enable

h41 to bind RIIα subunits, we endeavored to confirm the principal importance of h41 as the primary RIIα-binding interface using targeted point mutations (Fig. 4 *B* and *C*). The most common approach for this is substitution of one of the core hydrophobic residues with a helix-breaking proline [as seen in the inactive Ht31p control peptide (36)]. However, given the importance of individual talin α-helices in forming the helical bundles that establish R domain conformation and the importance of R9 in maintaining talin in an autoinhibited conformation (54), we wanted to avoid using a mutation with such a high likelihood of causing global and activating conformational changes. Overlay assays revealed that two mutants with conservative substitutions (V1807A and V1800A/V1807A) still bound RIIα D/D, albeit at a significantly reduced level, while a double mutant with more radical substitutions that disrupt the hydrophobic face of h41 but still support helicity (A1806D/V1807D) exhibited markedly reduced binding (Fig. 4*C*), confirming the importance of h41 for PKA RII binding. These results unequivocally establish h41 as the PKA RIIα-binding site in talin1.

The preceding observations demonstrate that h41 is the RIIα binding site and is available for PKA binding when it is "free" or unbundled, as in h41-R10 (Fig. 4*A*). However, in the context of the complete R9 domain bundle, the site is "cryptic" and requires unfolding of R9 and exposure of the hydrophobic face of h41 for
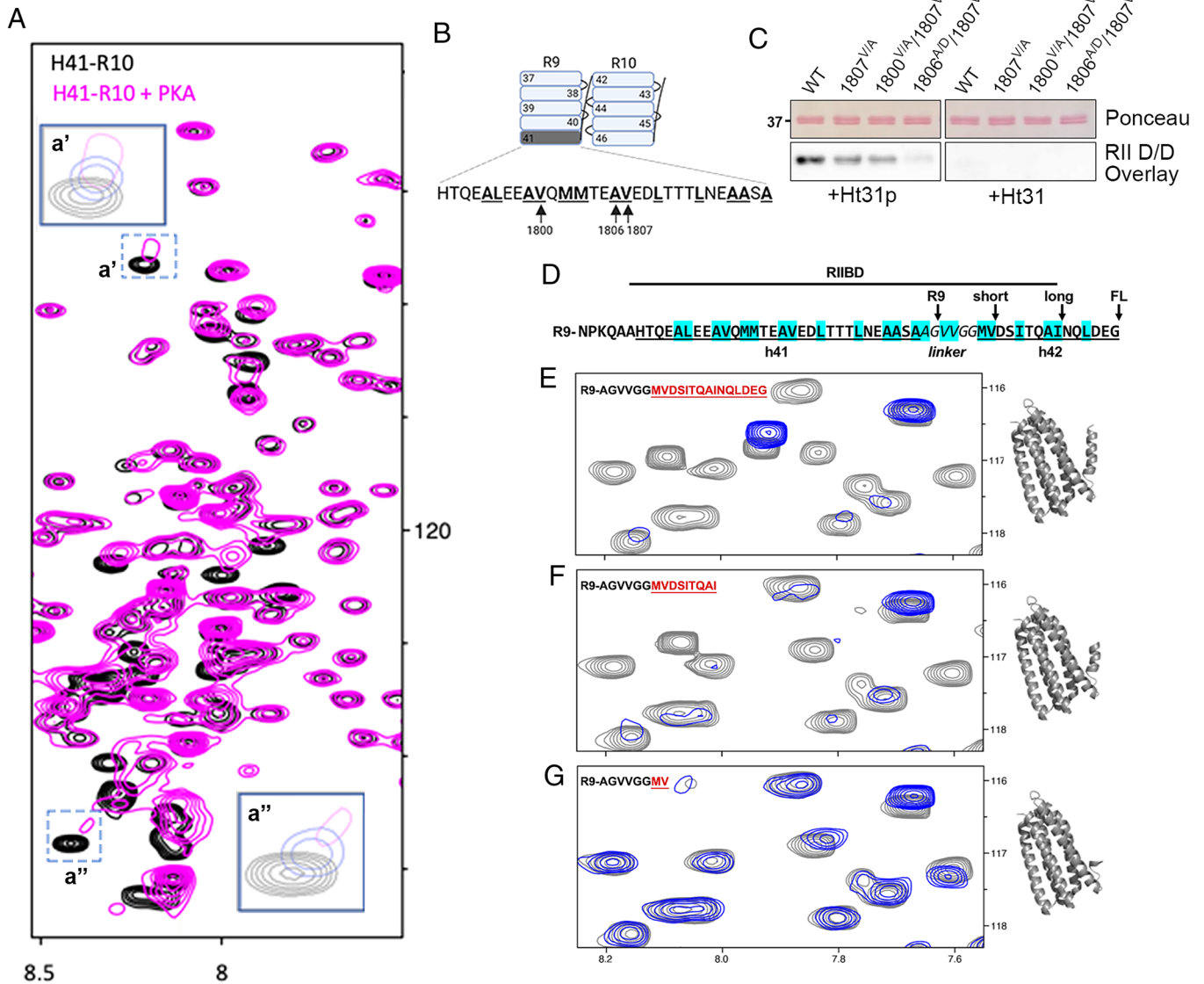
Fig. 4. Helix41, the R9-R10 linker, and part of helix42 together are required for PKA D/D RII binding. (*A*) ^{1}H,^{15}N-HSQC spectra of ^{15}N-labeled talin1 helix41-R10 (h41-R10; residues 1785 to 1973) in the absence (black) or presence (magenta) of PKA RIIα D/D domain at a ratio of 1:5. The intense peaks from h41 are the ones that shift. Two *Insets* (*a'*, *a''*) show magnification of regions (indicated by dotted outlines) with peaks that shift on addition of increasing amounts of PKA RIIα D/D (1:0, 1:3. 1:5 in black, blue, and magenta, respectively). (*B* and *C*) Three single or double point mutants, targeting selected hydrophobic residues within h41 (*B*), were generated and analyzed by PKA RIIα D/D domain overlay (*C*) (n = 2 experimental replicates). (*D*) Amino acid sequence of h41-linker-h42. Underlining indicates amino acids in helices, italics indicate the linker, and highlighting indicates hydrophobic residues. The terminus of R9-h42 (*FL*), long and short h42 truncations, and the R9 domain-only construct are indicated with arrows (RIIBD = RII binding domain). (*E–G*) ^{1}H,^{15}N-HSQC spectra of ^{15}N-labeled talin R9-h42 (*E*) and truncated [long (*F*), short (*G*)] fragments in the absence (gray peaks) or presence (blue peaks) of PKA RIIα D/D domain fragments at a ratio of 1:3. In each panel, the common linker is shown in black and the varying lengths of h42 are shown in red underline.

RIIα access (Fig. 3 *B–D*), which appears to require R10. Therefore, we wanted to determine how much of the R10 domain is required to unfold R9 and allow PKA to bind. Thus, we analyzed an ^{15}N-labeled talin1 fragment comprising R9-h42 (R9 through to the first full helix of R10; Fig. 4*D*) and found that addition of PKA RIIα D/D to R9-h42 elicited clear, striking changes in R9 spectral peaks, indicating that the addition of h42 alone was sufficient to allow PKA to unfold and bind to R9 (Fig. 4*E*). Thus, both h41-R10 and R9-h42 are able to bind PKA — one because the PKA binding site is constitutively exposed (h41-R10) and the other because PKA is able to unfold R9 to expose it (R9-h42).

To further define how much of the sequence beyond R9/h41 is required to allow PKA to unfold R9 and bind, we analyzed a series of fragments of R9-h42 (Fig. 4 *D–G*), with decreasing

lengths of the R9-R10 linker and h42 (Fig. 4*D*), approaching the R9 domain alone which is not unfolded by PKA (Fig. 3*D*). Thus, R9 with 13 additional residues (spanning the entire R9-R10 linker and first 10 of the 16 h42 residues; *R9-h42-long*) unfolded and bound to PKA RIIα D/D as efficiently as the full-length R9-h42 (Fig. 4*F*). However, R9 with only six additional residues (spanning the R9-R10 linker and first two h42 residues; *R9-h42-short*) showed only weak binding to PKA RIIα D/D and no unfolding of R9 (Fig. 4*G*). Recall that removal of these six residues generates R9 alone which, as shown above, does not bind (Fig. 3*D*). These data indicate that the interaction of PKA RIIα to talin1 is mediated by h41 in R9, but in a manner that requires the R9-R10 linker and a small portion of h42 in R10 for unfolding, exposure, and strong binding. Based on these cumulative data, we assign the

region of amino acids 1791 to 1835 (h41-linker-h42-long) as the talin1 PKA RII binding domain (RIIBD; Fig. 4D and *SI Appendix, Table S1*). Interestingly, the first six residues of the h42 sequence in R10, that are required for PKA binding to R9, are not a well-defined part of the helix in the structures containing R10 (52) which likely explains why PKA binding does not unfold, nor require unfolding of, R10.

Mechanical Force across Talin Regulates PKA RIIα Binding. At the nexus of ECM-bound integrins and the actomyosin cytoskeleton, talin1 functions not only as a linker but also as a mechanosensitive scaffold, with force-dependent unfolding of its rod domains controlling interactions with various binding partners (30, 31, 33). The most well-studied example of this mechanosensitivity is the binding of talin to vinculin, with elegant structural and biophysical studies establishing that this interaction requires unfolding of talin rod bundles containing cryptic VBS that can be attained in vitro by application of mechanical force across relevant talin rod domain fragments (32, 55–57). Given that PKA binding to talin1 requires the talin R9 domain to unfold, it has the potential to be similarly regulated by mechanical force. This would be consistent with the current observation that, while talin1 is one of the most abundant proteins biotinylated by RIIα-mTb, coimmunoprecipitation of talin1 with RIIα-mTb occurred only under crosslinking conditions (Fig. 2C).

To test this, we used magnetic tweezers to immobilize and mechanically stretch the talin1 R9-12 fragment, as described previously (58), to generate force-extension curves before and after addition of PKA RIIα D/D. For each force cycle, a linearly increasing force from 1.5 to ~30 pN is applied to the protein tether at a constant loading rate (2 pN/s) to unfold the domains, then the applied force is reduced to ~1.5 pN to allow refolding. During force loading, the height of the end-attached paramagnetic microbead is recorded at a nanometer resolution in real time (59, 60). In the absence of PKA RIIα D/D, R9–12 shows four distinct unfolding steps in the force range of ~10 to 25 pN (Fig. 5 *A* and *C*), with each extension of ~35 to 50 nm corresponding to the unfolding of one rod domain bundle as seen previously (58). These results confirm that, in the absence of other proteins, each domain unfolds rapidly once the applied force exceeds the mechanical stability of that domain and that they each faithfully refold at low forces.

Importantly, this characteristic force-bead height profile is significantly altered after addition of PKA RIIα D/D (Fig. 5 *B* and *D* and *SI Appendix, Fig. S9*). Specifically, in the first cycle in the presence of 100 nM PKA RIIα D/D, the characteristic four unfolding steps of R9-12 are still present, indicating that PKA addition alone was not sufficient to unfold the domains. However, within 1 to 2 force loading cycles, the number of unfolding steps decreased from four to three, and correspondingly the bead height increased at forces below 10 pN. Moreover, the three unfolding
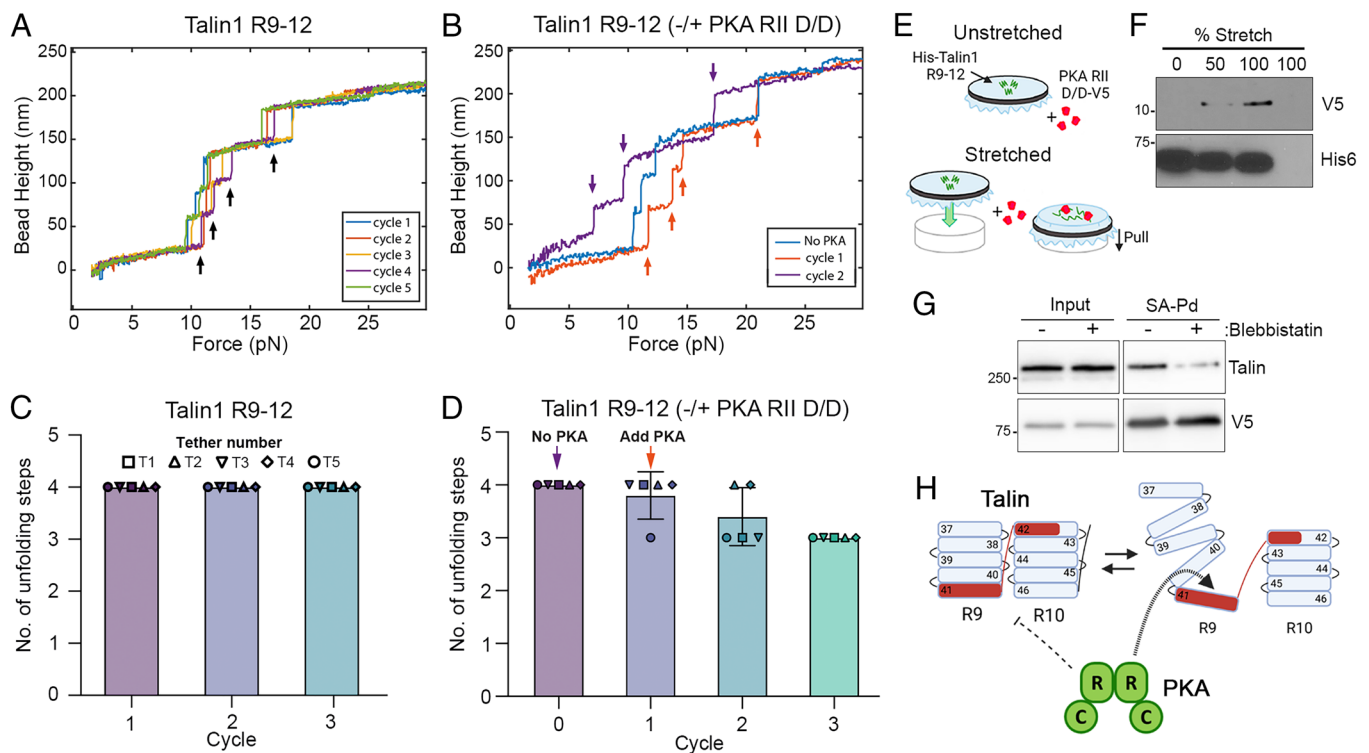

Fig. 5. Mechanical gating of talin-PKA interaction. (A–D) Magnetic tweezers were applied to immobilized, paramagnetic bead-conjugated Talin1 R9-12 to generate unfolding force *vs* bead height (i.e., extension) curves. (A) Iterative extension cycles of a single talin R9-12 tether, demonstrating four characteristic extensions corresponding to the unfolding of each of the four R domains (black arrows). Following each force-loading process, the tether was returned to and maintained at ~1.5 pN for 100 s to allow domains to refold before the next force-loading process. (B) Iterative cycles of a single talin R9-12 tether before (blue) and after (orange, purple) addition of 100 nM PKA RIIα D/D domain. The characteristic four unfolding steps persist for one extension cycle after addition of PKA D/D (orange arrows) but reduce to three (purple arrows) in the subsequent cycle, indicating unfolding-dependent binding of PKA RIIα D/D which inhibits the refolding of one domain. (C and D) The number of unfolding steps during consecutive force-loading processes for five independent tethers alone (C) or before and after addition of PKA D/D domain (D). (E) Schematic of the immobilized protein extension (IPE) assay. Bait protein, adsorbed onto a flexible silicon sheet which is left taught or stretched to varying extents, is incubated with prey protein and bound proteins are analyzed by immunoblotting. (F) IPE assays of uncoated or His$_6$(R9-12)-coated sheets that were unstretched (0%) or stretched by the indicated amounts (as % increase in surface area) before incubation with V5-tagged PKA RIIα D/D domain. Bound proteins were collected and immunoblotted with the indicated anti-tag antibodies. (G) V5-RIIα-mTb expressing cells were labeled with biotin in the absence or presence of 25 μM of blebbistatin. Lysates (Input) or biotinylated proteins isolated using streptavidin bead pull-down (SA-Pd) were immunoblotted with the indicated antibodies. (H) A hypothetical model of mechanically gated talin-PKA RII interaction where unfolding of the R9 domain leads to exposure of the talin AKAP motif and binding of PKA.

steps persisted in subsequent force-loading cycles (Fig. 5*D* and *SI Appendix,* Figs. S9 and S10), indicating that one domain was unable to refold. Interestingly, we sometimes observed a further reduction in the number of unfolding steps during subsequent force-loading cycles (*SI Appendix,* Fig. S10), implying that the bound PKA RIIα D/D may exert a suppressive effect on the refolding of adjacent domains as well. Together, these data indicate an unfolding-dependent binding of PKA RIIα D/D to talin R9-12 and subsequent inhibition of the refolding of one or more domains.

We noticed with some tethers that increased numbers of force loading cycles (typically 3 to 4 cycles) in the presence of RIIα D/D led to a reduction in the maximum extension length of R9-12 at the maximal tested force (*SI Appendix,* Fig. S11), suggesting the possibility of an additional interaction between PKA RIIα D/D and unfolded α-helices in R9-R12. However, such an additional interaction was not evident in our biochemical assays. We note that maintaining R9 in an unfolded state exposes two buried cysteines (C1661 and C1671), and even though the experiments were done in the presence of reducing agent (2 mM TCEP), we cannot exclude that this is not a result of looping via a disulfide bond that is only able to form because the R9 is prevented from refolding. Nonetheless, the reduced number of unfolding steps persisted through multiple force-loading cycles even as the maximum extension length decreased (Fig. 5*B* and *SI Appendix,* Figs. S10 and S11). Together, these observations unequivocally demonstrate the regulation of talin-PKA interaction by force-dependent changes in talin conformation and show that PKA RIIα D/D stabilizes the unfolded conformation of one of the domains through multiple cycles of force-loading.

We corroborated the observations from these single-molecule experiments using a previously described immobilized protein extension (IPE) assay (61) in which the talin1 R9-12 fragment was adsorbed onto a silicon membrane before incubation with RIIα D/D under unstretched or stretched conditions (Fig. 5*E*). While only qualitative, this assay clearly showed that RIIα D/D bound to immobilized talin1 R9-12 in proportion to the level of membrane stretch with minimal binding in the absence of stretch (Fig. 5*F*), further demonstrating direct mechanical regulation of the talin1-PKA interaction. Finally, we sought to further support these observations by altering actomyosin contractility in cells. Thus, we treated cells expressing RIIα-mTb with blebbistatin and then assessed the amount of talin recovered in streptavidin pull-downs. While the level of auto-biotinylated RIIα-mTb remained unchanged, indicating no contractility-dependent changes in ligase activity, the level of talin in the blebbistatin-treated sample was significantly reduced (Fig. 5*G*). These data are consistent with a blebbistatin-induced reduction of contractility leading to decreased mechanical unfolding of talin1 (62) and reduction in talin1 biotinylation through decreased tension-dependent binding of PKA RIIα-mTb. These observations establish that talin binds directly to PKA and that the talin-PKA interaction is regulated by conformational changes in talin that are controlled by mechanical force (Fig. 5*H*).

Talin Anchors PKA to FA In Vivo. To determine whether talin actually functions as an AKAP in cells, we generated stable human umbilical vein endothelial cells (HUVECs) expressing GFP-tagged WT talin1 or the PKA nonbinding A1806D/V1807D ("AV/DD") mutant described in Fig. 4*C*. Whereas most cell types express talin1 as well as the closely-related talin2 isoform, HUVECs express only talin1, so the phenotypes associated with loss of endogenous talin1 are not compensated by talin2 but can be rescued by expression of exogenous talin1 (63). Thus, we serially transduced HUVECs first with lentivirus encoding GFP-tagged WT or AV/DD murine talin1 and then a second lentivirus expressing shRNA against

human talin1. Immunoblotting confirmed both knockdown of endogenous talin1 and reexpression of the GFP-tagged isoforms (Fig. 6*A*). Recent work has shown that PKA RIIα subunits are retained in FAs in unroofed cells (24). Moreover, phospho-Ser99 RII, which is part of an epitope that is exposed upon dissociation of the PKA C subunit following enzyme activation and is used as a readout of PKA activity within the anchored holoenzyme (64, 65), is enriched in FAs (24). Immunofluorescence analysis showed the localization of both total and active (i.e., phospho-Ser99) RIIα in GFP-positive FAs is significantly reduced in sh-AV/DD-talin HUVECs compared to sh-WT-talin cells (Fig. 6 *B–E*). These data confirm that talin is a bona fide AKAP that contributes to localization of PKA to FAs.

We sought to determine whether loss of talin-mediated PKA anchoring exhibited effects on FA signaling or function. However, while the AV/DD mutation effectively disrupts talin-RII interaction (Fig. 4*C*), it still can also alter helical bundling within R9 which may affect talin conformation which may, in turn, have effects on FA dynamics that are independent of loss of AKAP function. Therefore, we endeavored to assess a readout more "proximal" to the loss of PKA function within FAs by measuring the relative phosphorylation of VASP (vasodilator-stimulated phosphoprotein)—a FA protein with important scaffolding and actin-regulatory roles and a known substrate for PKA (66)—within FAs in sh-WT and sh-AV/DD HUVECs. Coimmunofluorescence with antibodies against total VASP and against VASP phosphorylated on Ser157 [the preferred PKA site (66)] allowed ratiometric measurement of relative VASP phosphorylation within individual, GFP-talin-positive FAs (Fig. 6*F*) and revealed a significant decrease in phospho-VASP in AV/DD-talin adhesions compared to WT (Fig. 6 *F* and *G*). These data demonstrate that mutations that disrupt talin-PKA RII interaction in vitro result in decreased PKA abundance and activity in FAs in vivo. Together, the observations in this report establish talin as a conformationally regulated AKAP that contributes to localizing PKA activity within FAs.

Discussion

It is clear that cellular signal transduction events often occur through multiprotein scaffolds that consolidate, localize, and specify signaling inputs and outputs (4, 67). There is increasing recognition that proteins involved in cell–ECM adhesion are ideally positioned to convert mechanical force into altered biochemistry (68, 69). This report bridges these two important fields by identifying talin, the archetypal FA protein, as a mechanically-gated anchoring protein for PKA. In so doing, it also establishes PKA, a pleiotropic kinase with myriad cellular targets, as a force-dependent binding partner and signal transducer for talin. Together, these observations form the foundation for a mechanotransduction pathway that utilizes force-dependent changes in protein conformation to establish a new, solid-state signaling complex well positioned to couple cellular tension to cellular communication.

Given the promiscuity of PKA activity and the number and diversity of substrates, mechanisms have evolved to focus PKA function to enhance signaling fidelity and specificity. The best-characterized mechanism for this is through AKAP-mediated changes in PKA localization, thereby sequestering PKA activity to specific subcellular niches, substrates, and events (4, 10, 13). The diversity of mammalian AKAP complexes, which differ not only in their localization but also in their composition and dynamics, produces a wide range of distinct signalosomes, each producing highly regulated and specific outputs. Thus, identifying new AKAPs increases our understanding not only of how PKA contributes to
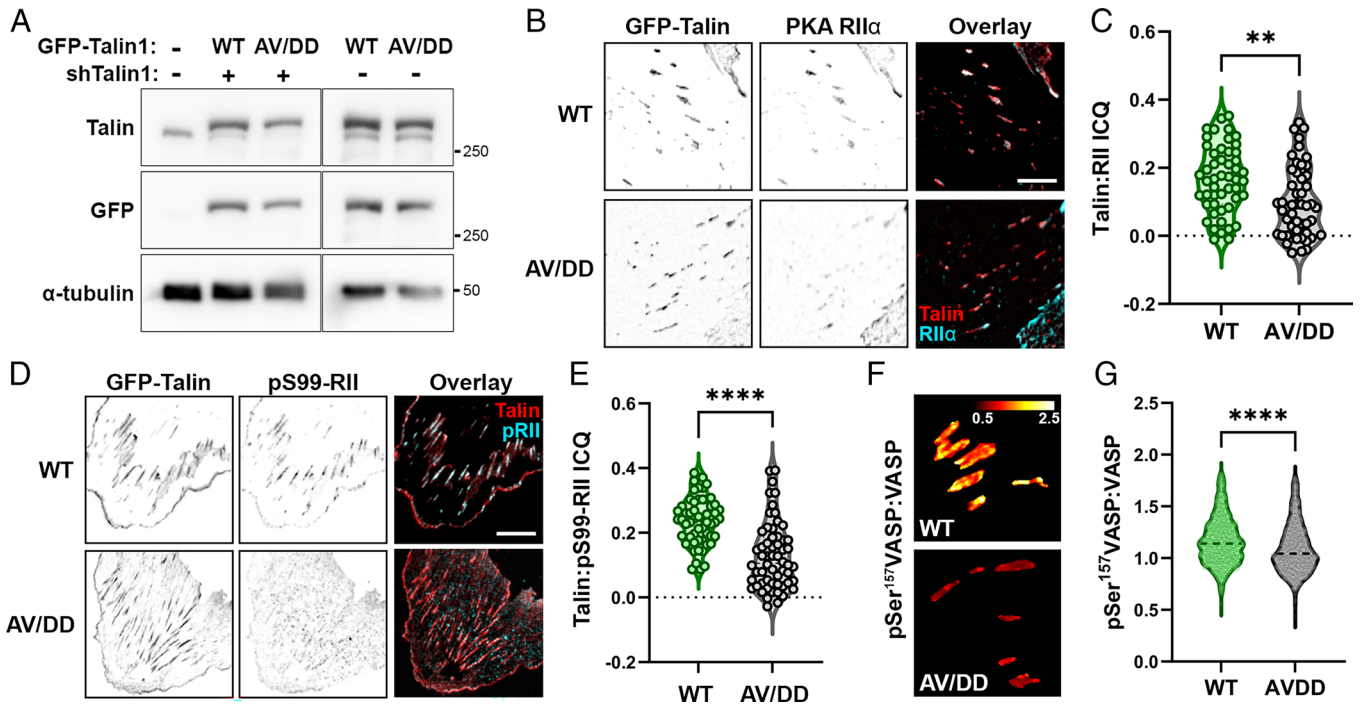
Fig. 6. Mutation of the PKA binding site in talin-1 decreases levels of PKA RIIα subunits, phosphorylated RII, and VASP phosphorylation in focal adhesions. (*A*) HUVECs were serially transduced with lentivirus expressing GFP-tagged murine wild-type (WT) or PKA nonbinding A^{1806}D/V^{1807}D talin (AV/DD) and lentivirus expressing shRNA against human talin-1, then analyzed by immunoblotting with the indicated antibodies. (*B*) Stable, sh-WT or sh-AV/DD cells plated on FN-coated coverslips, then fixed, unroofed, and immunostained to visualize PKA RIIα in GFP-positive adhesions (Scale bar: 10 µm.) (*C*) Intensity correlation quotients (ICQ) were determined to quantify colocalization of talin and RIIα in WT and AV/DD cells (from 50 full-frame microscopic fields from three separate experiments; **P < 0.05). (*D*) Stable sh-WT or sh-AV/DD cells were processed as in (*B*) and immunostained to visualize active, phospho-Ser99 PKA RII (pS99-RII) in GFP-positive adhesions. (*E*) Quantification of colocalization of talin and pS99-RII PKA in WT and AV/DD cells (from 58 full-frame microscopic fields from three separate experiments; ****P < 0.001). (*F*) Stable sh-WT or sh-AV/DD cells were processed as in (*B*), stained with antibodies against total VASP and VASP phosphorylated on Ser157 (pSer^{157}VASP), and ratiometric images of phospho-VASP to total VASP were generated as described in *Materials and Methods* (panels depict a 15 × 15 µm region of interest). (*G*) Quantification of pSer^{157}VASP:VASP ratios from 1,078 and 1,073 individual WT or AV/DD adhesions, respectively, from three separate experiments. Violin plots show all data points, with dotted lines indicating mean values (1.169 and 1.091 for WT and AV/DD, respectively; ****P < 0.001).

specific cellular events but also of how signaling is controlled at the subcellular scale. In this way, the current demonstration of talin as an AKAP provides an important new niche for PKA signaling, while the demonstration that the PKA–talin interaction is regulated by mechanical force across talin establishes an important new way to regulate PKA anchoring.

The current data show direct, mechanical gating of PKA anchoring. Indeed, a requirement for conformational rearrangement for AKAP-PKA interaction is not common—nearly all known AKAPs are reported to interact with PKA R subunits constitutively (36, 70, 71). To our knowledge, the only other exception is ezrin, a membrane-cytoskeleton adapter whose phosphorylation-dependent switch between open and closed conformations controls its binding to PKA type-I, but not RIIα, subunits (51, 72). The PKA binding site in talin identified here is similarly cryptic, being occluded when R9 is in its closed conformation and available for binding only when the domain is opened—by denaturation and partial refolding (as in the overlay assays), high stoichiometric excess of PKA D/D domain (as in the NMR assays), or mechanical extension through applied force (Fig. 5 *A–F*). Furthermore, the PKA binding domain in h41 of talin has some divergence from canonical RIIα binding motifs [Fig. 4 *B* and *D* and *SI Appendix,* Fig. S5, and (4, 36, 43)]. While notable, this divergence is not as radical as seen in pericentrin, a centrosomal protein that anchors PKA through a large, noncanonical domain of ~85 amino acids that is rich in leucine and valine repeats, is not predicted to form an amphipathic helix, and exhibits no significant sequence or structural homology to the RII binding sequence in talin identified here (73). Nonetheless, the requirement for mechanical gating for

talin-PKA interaction, combined with the slight divergence of talin h41 from canonical RIIα binding motifs, underscores the uniqueness of the PKA–talin complex and importance of determining its structural detail at higher resolution—a pursuit currently underway. It further suggests the possibility of additional, "semicanonical" AKAPs with divergent binding motifs that might not be readily predicted by in silico algorithms. It is therefore tempting to posit the possibility of additional mechanically regulated PKA anchors in other dynamic, tension-bearing cellular structures such as cell–cell junctions and kinetochores.

The mechanically regulated interaction between PKA and talin also has important consequences for our understanding of talin biology. Talin binds other enzymes [*e.g.,* focal adhesion kinase, phosphatidylinositol 4-phosphate 5-kinase type I-γ, cyclin-dependent kinase-1 and alpha tubulin acetyltransferase 1 (30, 47, 74)] but the talin-PKA interaction is noteworthy because it represents a report of an enzyme that binds preferentially to a mechanically opened rod domain. Previously, the only other protein known to bind to the force-dependent open conformation of talin rod domains was vinculin, another core actin-binding FA protein and mechanotransducer (30, 32, 75, 76). Indeed, there are important parallels between the well-known, mechanically regulated talin–vinculin interaction and the newly described talin-PKA interaction. Each of the 11 VBS in talin consists of a string of hydrophobic residues along the face of an individual helix buried within the folded rod domains. For talin–vinculin interaction, force across the talin rod exposes one or more of these sites, recruiting vinculin to FAs and strengthening the link between integrins and F-actin (30, 75–77). As only 11 of the 62 helices that form the 13 talin rod domains

have been reported to bind vinculin once exposed, the remaining helices might also be expected to bind other ligands, yet evidence for this has been lacking until now. Therefore, the PKA–talin interaction confirms a new paradigm for talin signaling whereby signaling molecules and enzymes can be directly recruited to the exposed residues of open talin domains.

While not likely to contribute to architectural reinforcement directly, it is quite likely that recruitment of PKA to talin may, as a proximal effect, promote the phosphorylation of talin itself and/or some of the myriad talin-associated proteins (30, 31, 78). Circumstantial, but nonetheless supportive, evidence for this comes from the presence of predicted PKA phosphorylation sites in talin and several talin-associated proteins (using PhosphoSitePlus, Phosida, and dbPAF; also ref. 79) and the presence of talin and interactors in unbiased screens for PKA substrates (80–86). The current demonstration of decreased phosphorylation of VASP in FA from cells expressing an AKAP-deficient mutant of talin expands this hypothesis. While VASP is associated with talin, this interaction is indirect—mediated through the adapter protein RIAM—and is thought to occur only in nascent adhesions and not mature FAs (30, 87), as analyzed here. Nonetheless, VASP is a prominent FA protein and has important, complex roles as a scaffold and regulator of microfilament dynamics during cell migration (66). VASP phosphorylation is similarly complex, occurring on at least three sites and potentially mediated by several kinases including PKA (66, 88). The most common effect of phosphorylation at Ser 157 is regulation of VASP protein–protein interactions (e.g., with various SH3-domain-containing proteins) but the consequences of this for VASP function and adhesion and migration dynamics are not fully understood (66, 88). While other kinases can phosphorylate VASP Ser157 (66, 88), none are known to interact with talin or to be immediate effectors of PKA, so it is reasonable to conclude that the decrease in Ser157 phosphorylation in FAs containing AKAP-deficient talin is likely due to loss of local PKA activity. Thus, this modification serves as a useful readout of local PKA activity in FAs, and this may provide a foundation for deeper understanding of VASP function and regulation. Finally, given the dense, layered, and multicomponent composition of FAs (28), it is reasonable to expect that talin-anchored PKA might phosphorylate additional proteins that do not directly interact with talin but are nonetheless present in FAs (11, 13, 24). Identification of substrates for the talin-anchored pool of PKA and characterization of the effects and consequences of their phospho-regulation is an important and likely fruitful endeavor.

Another important direction for future efforts involves delineating the cellular regulation and function of the talin-PKA complex. Talin is autoinhibited by interaction between R9 and the F3 domain in the talin head; as F3 contains the principal integrin binding site of talin, this interaction must be released to allow binding to actin and integrin and recruitment to FAs (30, 31, 78). We have shown that the major constituent of the PKA binding site in talin is h41 of R9, which therefore suggests that the talin-PKA interaction is most likely to occur at sites of talin activation where R9 is unfolded. Similarly, PKA binding to talin might limit R9 refolding, maintaining talin in an active conformation, and so activate and sustain adhesion assembly. Direct analysis of the force borne by talin in adhesive complexes in live cells, using a mechanically responsive talin biosensor, established that talin is under higher tension in peripheral FAs compared to more central FAs and/or fibrillar adhesions, and even showed heterogenous force-loading within individual FAs (62, 89). In recent work, we have reported that PKA is active and dynamic within

subregions of FA (24). Furthermore, as the opening of talin rod domains introduces 40 to 50 nm extension in the length of the talin molecule (90), the anchoring of PKA could be dynamically moved within each adhesion as other talin rod domains open and close. It will be an informative challenge to determine the precise subset of adhesion complexes (or subregions within individual adhesion complexes) in which the talin-PKA interaction occurs.

Finally, it will also be important to identify the physiological function of talin-mediated PKA anchoring for cell adhesion and motility. Recent work demonstrated that global inhibition of PKA during cell spreading promotes an adhesive phenotype characterized by elongated, clustered FAs located along the cell periphery with fewer, smaller adhesions in the cell center (24). While this phenotype may involve PKA-dependent pathways outside of the FA structure itself, it suggests that PKA may be involved in regulating the assembly, maturation, and/or turnover of FAs. In this regard, it is noteworthy that longitudinal "splitting" and maturation of FA clusters into individual adhesions requires VASP (91) and that depletion of VASP—phosphorylation of which is regulated by talin-anchored PKA (Fig. 6)—prevents splitting and results in FA clusters similar to those seen in PKA-inhibited cells (24, 91). Similarly, DLC1, a talin-associated Rho GAP (92, 93), localizes to mature FAs (94), increases FA lifetime (94), and is regulated by PKA (95). DLC1 also interacts with tensin-3 (96), a prominent component of integrin-associated fibrillar adhesions that mature from FAs in the cell center and are associated with ECM fibrillogenesis (97). Notably, tensin-3 drives the formation of fibrillar adhesions in a manner dependent on its interaction with talin (98) and has also recently been identified as a novel PKA substrate (24). While circumstantial, these observations support not only the hypothesis that PKA may have complex roles in FA dynamics and maturation but also the assertion that there may be many individual targets or multiprotein complexes regulated through anchoring of PKA to talin.

Ultimately, the task of parsing the roles of talin-anchored PKA in FA dynamics will require the generation of discrete talin point mutants that prevent RIIα binding without altering any other talin function (e.g., talin autoinhibition, folding/refolding; other protein–protein interactions). Although we show here it is possible to disrupt the talin-PKA interaction using a canonical AV/DD (A^{1806}D/V^{1807}D) mutant, this mutant is limited in its utility as it results in constitutive unfolding of the R9 domain, which would also prevent talin regulation by autoinhibition. While the goal of identifying a discrete AKAP-deficient mutant will be greatly facilitated by higher resolution analysis of the unique structure of the talin-RIIα complex, more immediate empirical efforts may be informed by analysis of talin mutants that are analogous to single nucleotide polymorphisms in known AKAPs that spare α-helix formation but significantly reduce PKA-binding (53). While there is much work to be done, this report establishes an important new protein–protein interaction that impacts our understanding of PKA localization, talin function, and mechanotransduction.

Materials and Methods

ImageJ macros are available from https://github.com/howelabuvm/Kang_PNAS2024 (99).

Focal Adhesion Cytoskeletal (FACS) Complex Preparation. FACS complexes were prepared using a modification of the method (100) in which cells are fixed with a reversible crosslinker, permeabilized, then unroofed by hydrodynamic shear. FACS proteins are collected, reverse-crosslinked, acetone precipitated,

resuspended, and used immediately for FA AKAP screening or stored at −20 °C for further analyses.

Focal Adhesion AKAP Screening. RIIα-mTb cells were grown with or without 2 µg/mL doxycycline for 18 h until ~70% confluency, followed by incubation with 50 µM biotin-containing media for 3 h. FACS proteins were collected from the non- or Dox-treated cells and diluted in RIPA buffer (Millipore). Biotinylated proteins were isolated by streptavidin pull-down (SA-Pd) using SA-coated magnetic beads (Invitrogen). The biotin-labeled proteins were separated by SDS-PAGE, trypsinized, and analyzed by LC/MS-MS (UVM Proteomics Core).

RII Overlay. First, 1.5 µg of recombinant proteins or 10 µg of U2OS WCE or FACS proteins were separated by SDS-PAGE and transferred to nitrocellulose. Blots were blocked with 10% nonfat dry milk (NFDM) in TBS-T for 1 h and then incubated with either V5-tagged PKA RIIα-D/D domain or full-length PKA RIIα (0.2 µg/mL concentration in 10% NFDM, containing either 0.4 µM Ht31p or Ht31 peptides) for 12 h. Then, after extensive washing with TBS-T, membranes were incubated with V5-HRP (BioLegend, 1:4,000 in 10% NFDM) for 12 h, washed with TBS-T, and developed by enhanced chemiluminescence.

NMR Analysis. ^{15}N-labeled protein samples were prepared at 150 µM final concentration in 12 mM NaH$_2$PO$_4$, 6 mM Na$_2$HPO$_4$, pH 6.5, 50 mM NaCl, 2 mM DTT, and 5%(v/v) D$_2$O. NMR spectra were collected at 298 K on Bruker Avance III 600 MHz NMR spectrometer equipped with CryoProbe. All data were processed via TopSpin and analyzed with CCPN analysis (101).

Single-Molecule Manipulation. These experiments were carried out as described previously (58), using a custom high-force magnetic tweezers platform that can exert forces up to 100 pN with ~1 nm extension resolution (59, 60). Talin R9-12 fragments were immobilized on the glass coverslip of a laminar flow chamber via using Halo-tag/Halo-ligand chemistry and tethered to a 3-mm paramagnetic bead through biotin/streptavidin chemistry.

Generation of Transduced HUVEC Lines. WT and AV/DD GFP-talin1 sequences were cloned into pLVX-IRES-Hygro-RGECO1.2 (Addgene, #164592), replacing the RGECO1.2 sequence through Gibson assembly. Pooled primary HUVECs (in ECGM2 growth media, both from PromoCell) were transduced with GFP-tagged WT or AV/DD talin1 lentiviruses and selected for 7 d in 100 µg/mL of hygromycin. Pooled resistant cells were transduced with lentivirus particles expressing a puromycin-resistance marker and shRNA against human talin1 (sc-36610-V; Santa Cruz Biotechnology). HUVEC^{shWT} and HUVEC$^{shAV/DD}$ lines were selected and maintained in ECGM2 containing 100 µg/mL of hygromycin and 1 µg/mL puromycin.

Data, Materials, and Software Availability. All study data are included in the article and/or supporting information.

Author affiliations: ᵃDepartment of Pharmacology, University of Vermont Larner College of Medicine, Burlington, VT 05405; ᵇDepartment of Molecular Physiology and Biophysics, University of Vermont Larner College of Medicine, Burlington, VT 05405; ᶜUniversity of Vermont Cancer Center, Burlington, VT 05405; ᵈSchool of Biosciences, University of Kent, Canterbury, Kent CT2 7NJ, United Kingdom; ᵉDepartment of Biochemistry, Cell and Systems Biology, Institute of Systems, Molecular and Integrative Biology, University of Liverpool, Liverpool L69 7ZB, United Kingdom; and ᶠDepartment of Physics, Mechanobiology Institute, National University of Singapore, Singapore 117542, Singapore

1. S. S. Taylor *et al.*, Dynamics of signaling by PKA. *Biochim. Biophys. Acta* **1754**, 25–37 (2005).
2. J. B. Shabb, Physiological substrates of cAMP-dependent protein kinase. *Chem. Rev.* **101**, 2381–2411 (2001).
3. N. Patel, M. G. Gold, The genetically encoded tool set for investigating cAMP: More than the sum of its parts. *Front Pharmacol.* **6**, 164 (2015).
4. J. D. Scott, C. W. Dessauer, K. Tasken, Creating order from chaos: Cellular regulation by kinase anchoring. *Annu. Rev. Pharmacol. Toxicol.* **53**, 187–210 (2013).
5. J. F. Zhang, S. Mehta, J. Zhang, Signaling microdomains in the spotlight: Visualizing compartmentalized signaling using genetically encoded fluorescent biosensors. *Annu. Rev. Pharmacol. Toxicol.* **61**, 587–608 (2021).
6. F. D. Smith *et al.*, Local protein kinase A action proceeds through intact holoenzymes. *Science* **356**, 1288–1293 (2017).
7. F. D. Smith *et al.*, Intrinsic disorder within an AKAP-protein kinase A complex guides local substrate phosphorylation. *Elife* **2**, e01319 (2013).
8. S. E. Tillo *et al.*, Liberated PKA catalytic subunits associate with the membrane via myristoylation to preferentially phosphorylate membrane substrates. *Cell Rep.* **19**, 617–629 (2017).
9. R. Walker-Gray, F. Stengel, M. G. Gold, Mechanisms for restraining cAMP-dependent protein kinase revealed by subunit quantitation and cross-linking approaches. *Proc. Natl. Acad. Sci. U.S.A.* **114**, 10414–10419 (2017).
10. P. Skroblin, S. Grossmann, G. Schafer, W. Rosenthal, E. Klussmann, Mechanisms of protein kinase A anchoring. *Int. Rev. Cell Mol. Biol.* **283**, 235–330 (2010).
11. A. K. Howe, Regulation of actin-based cell migration by cAMP/PKA. *Biochim. Biophys. Acta* **1692**, 159–174 (2004).
12. A. K. Howe, Cross-talk between calcium and protein kinase A in the regulation of cell migration. *Curr. Opin. Cell Biol.* **23**, 554–561 (2011).
13. K. V. Svec, A. K. Howe, Protein kinase A in cellular migration-Niche signaling of a ubiquitous kinase. *Front Mol. Biosci.* **9**, 953093 (2022).
14. A. K. Howe, L. C. Baldor, B. P. Hogan, Spatial regulation of the cAMP-dependent protein kinase during chemotactic cell migration. *Proc. Natl. Acad. Sci. U.S.A.* **102**, 14320–14325 (2005).
15. A. J. McKenzie, S. L. Campbell, A. K. Howe, Protein kinase A activity and anchoring are required for ovarian cancer cell migration and invasion. *PLoS One* **6**, e26552 (2011).
16. A. J. McKenzie, K. V. Svec, T. F. Williams, A. K. Howe, Protein kinase A activity is regulated by actomyosin contractility during cell migration and is required for durotaxis. *Mol. Biol. Cell* **31**, 45–58 (2020).
17. D. Gau, W. Veon, S. G. Shroff, P. Roy, The VASP-profilin1 (Pfn1) interaction is critical for efficient cell migration and is regulated by cell-substrate adhesion in a PKA-dependent manner. *J. Biol. Chem.* **294**, 6972–6985 (2019).
18. P. Gui *et al.*, Integrin receptor activation triggers converging regulation of Cav1.2 calcium channels by c-Src and protein kinase A pathways. *J. Biol. Chem.* **281**, 14015–14025 (2006).
19. A. K. Howe, B. P. Hogan, R. L. Juliano, Regulation of vasodilator-stimulated phosphoprotein phosphorylation and interaction with Abl by protein kinase A and cell adhesion. *J. Biol. Chem.* **277**, 38121–38126 (2002).
20. A. K. Howe, R. L. Juliano, Regulation of anchorage-dependent signal transduction by protein kinase A and p21-activated kinase. *Nat. Cell Biol.* **2**, 593–600 (2000).
21. C. J. Lim *et al.*, Integrin-mediated protein kinase A activation at the leading edge of migrating cells. *Mol. Biol. Cell* **19**, 4930–4941 (2008).
22. J. D. Whittard, S. K. Akiyama, Positive regulation of cell-cell and cell-substrate adhesion by protein kinase A. *J. Cell Sci.* **114**, 3265–3272 (2001).
23. M. G. Yeo *et al.*, Phosphorylation of Ser 21 in Fyn regulates its kinase activity, focal adhesion targeting, and is required for cell migration. *J. Cell Physiol.* **226**, 236–247 (2011).
24. M. Kang *et al.*, Protein kinase A is functional component of focal adhesions. bioRxiv [Preprint] (2023). https://doi.org/10.1101/2023.08.18.553932 (Accessed 2 March 2024).
25. K. Burridge, K. Fath, T. Kelly, G. Nuckolls, C. Turner, Focal adhesions: Transmembrane junctions between the extracellular matrix and the cytoskeleton. *Annu. Rev. Cell Biol.* **4**, 487–525 (1988).
26. M. A. Schwartz, Integrins and extracellular matrix in mechanotransduction. *Cold Spring Harbor Perspect. Biol.* **2**, a005066 (2010).
27. Z. Sun, S. S. Guo, R. Fassler, Integrin-mediated mechanotransduction. *J. Cell Biol.* **215**, 445–456 (2016).
28. P. Kanchanawong, D. A. Calderwood, Organization, dynamics and mechanoregulation of integrin-mediated cell-ECM adhesions. *Nat. Rev. Mol. Cell Biol.* **24**, 142–161 (2023).
29. B. Geiger, J. P. Spatz, A. D. Bershadsky, Environmental sensing through focal adhesions. *Nat. Rev. Mol. Cell Biol.* **10**, 21–33 (2009).
30. D. A. Calderwood, I. D. Campbell, D. R. Critchley, Talins and kindlins: Partners in integrin-mediated adhesion. *Nat. Rev. Mol. Cell Biol.* **14**, 503–517 (2013).
31. B. T. Goult, J. Yan, M. A. Schwartz, Talin as a mechanosensitive signaling hub. *J. Cell Biol.* **217**, 3776–3784 (2018).
32. A. del Rio *et al.*, Stretching single talin rod molecules activates vinculin binding. *Science* **323**, 638–641 (2009).
33. B. T. Goult, N. H. Brown, M. A. Schwartz, Talin in mechanotransduction and mechanomemory at a glance. *J. Cell Sci.* **134**, jcs258749 (2021).
34. M. Yao *et al.*, Mechanical activation of vinculin binding to talin locks talin in an unfolded conformation. *Sci. Rep.* **4**, 4610 (2014).
35. G. C. Mo *et al.*, Genetically encoded biosensors for visualizing live-cell biochemical activity at super-resolution. *Nat. Methods* **14**, 427–434 (2017).
36. M. G. Gold *et al.*, Molecular basis of AKAP specificity for PKA regulatory subunits. *Mol. Cell* **24**, 383–395 (2006).
37. T. C. Branon *et al.*, Efficient proximity labeling in living cells and organisms with TurboID. *Nat. Biotechnol.* **36**, 880–887 (2018).
38. J. D. Humphries *et al.*, Proteomic analysis of integrin-associated complexes identifies RCC2 as a dual regulator of Rac1 and Arf6. *Sci. Signal* **2**, ra51 (2009).
39. J. C. Kuo, X. Han, C. T. Hsiao, J. R. Yates IIIrd, C. M. Waterman, Analysis of the myosin-II-responsive focal adhesion proteome reveals a role for beta-Pix in negative regulation of focal adhesion maturation. *Nat. Cell Biol.* **13**, 383–393 (2011).
40. H. B. Schiller, C. C. Friedel, C. Boulegue, R. Fassler, Quantitative proteomics of the integrin adhesome show a myosin II-dependent recruitment of LIM domain proteins. *EMBO Rep.* **12**, 259–266 (2011).
41. R. Zaidel-Bar, S. Itzkovitz, A. Ma'ayan, R. Iyengar, B. Geiger, Functional atlas of the integrin adhesome. *Nat. Cell Biol.* **9**, 858–867 (2007).

42. P. P. Burgers, M. A. van der Heyden, B. Kok, A. J. Heck, A. Scholten, A systematic evaluation of protein kinase A–A-kinase anchoring protein interaction motifs. *Biochemistry* **54**, 11–21 (2015).

43. Z. E. Hausken, M. L. Dell'Acqua, V. M. Coghlan, J. D. Scott, Mutational analysis of the A-kinase anchoring protein (AKAP)-binding site on RII. Classification Of side chain determinants for anchoring and isoform selective association with AKAPs. *J. Biol. Chem.* **271**, 29016–29022 (1996).

44. R. L. Rivard, M. Birger, K. J. Gaston, A. K. Howe, AKAP-independent localization of type-II protein kinase A to dynamic actin microspikes. *Cell Motil Cytoskeleton* **66**, 693–709 (2009).

45. K. Dodge, J. D. Scott, AKAP79 and the evolution of the AKAP model. *FEBS Lett.* **476**, 58–61 (2000).

46. B. T. Goult *et al.*, Structural studies on full-length talin1 reveal a compact auto-inhibited dimer: Implications for talin activation. *J. Struct. Biol.* **184**, 21–32 (2013).

47. R. E. Gough *et al.*, Talin mechanosensitivity is modulated by a direct interaction with cyclin-dependent kinase-1. *J. Biol. Chem.* **297**, 100837 (2021).

48. D. B. Bregman, N. Bhattacharyya, C. S. Rubin, High affinity binding protein for the regulatory subunit of cAMP-dependent protein kinase II-B. Cloning, characterization, and expression of cDNAs for rat brain P150. *J. Biol. Chem.* **264**, 4648–4656 (1989).

49. S. M. Lohmann, P. DeCamilli, I. Einig, U. Walter, High-affinity binding of the regulatory subunit (RII) of cAMP-dependent protein kinase to microtubule-associated and other cellular proteins. *Proc. Natl. Acad. Sci. U.S.A.* **81**, 6723–6727 (1984).

50. D. W. Carr, Z. E. Hausken, I. D. Fraser, R. E. Stofko-Hahn, J. D. Scott, Association of the type II cAMP-dependent protein kinase with a human thyroid RII-anchoring protein. Cloning and characterization of the RII-binding domain. *J. Biol. Chem.* **267**, 13376–13382 (1992).

51. D. T. Dransfield *et al.*, Ezrin is a cyclic AMP-dependent protein kinase anchoring protein. *EMBO J.* **16**, 35–43 (1997).

52. B. T. Goult *et al.*, The domain structure of talin: Residues 1815–1973 form a five-helix bundle containing a cryptic vinculin-binding site. *FEBS Lett.* **584**, 2237–2241 (2010).

53. F. D. Smith *et al.*, Single nucleotide polymorphisms alter kinase anchoring and the subcellular targeting of A-kinase anchoring proteins. *Proc. Natl. Acad. Sci. U.S.A.* **115**, E11465–E11474 (2018).

54. B. T. Goult *et al.*, The structure of an interdomain complex that regulates talin activity. *J. Biol. Chem.* **284**, 15097–15106 (2009).

55. I. Fillingham *et al.*, A vinculin binding domain from the talin rod unfolds to form a complex with the vinculin head. *Structure* **13**, 65–74 (2005).

56. V. P. Hytönen, V. Vogel, How force might activate talin's vinculin binding sites: SMD reveals a structural mechanism. *PLoS Comput. Biol.* **4**, e24 (2008).

57. E. Papagrigoriou *et al.*, Activation of a vinculin-binding site in the talin rod involves rearrangement of a five-helix bundle. *Embo J.* **23**, 2942–2951 (2004).

58. M. Yao *et al.*, The mechanical response of talin. *Nat. Commun.* **7**, 11966 (2016).

59. X. Zhao, X. Zeng, C. Lu, J. Yan, Studying the mechanical responses of proteins using magnetic tweezers. *Nanotechnology* **28**, 414002 (2017).

60. H. Chen *et al.*, Improved high-force magnetic tweezers for stretching and refolding of proteins and short DNA. *Biophys. J.* **100**, 517–523 (2011).

61. Y. Sawada *et al.*, Force sensing by mechanical extension of the Src family kinase substrate p130Cas. *Cell* **127**, 1015–1026 (2006).

62. A. Kumar *et al.*, Talin tension sensor reveals novel features of focal adhesion force transmission and mechanosensitivity. *J. Cell Biol.* **213**, 371–383 (2016).

63. P. M. Kopp *et al.*, Studies on the morphology and spreading of human endothelial cells define key inter- and intramolecular interactions for talin1. *Eur. J. Cell Biol.* **89**, 661–673 (2010).

64. J. Isensee *et al.*, PKA-RII subunit phosphorylation precedes activation by cAMP and regulates activity termination. *J. Cell Biol.* **217**, 2167–2184 (2018).

65. M. H. Omar *et al.*, Mislocalization of protein kinase A drives pathology in Cushing's syndrome. *Cell Rep.* **40**, 111073 (2022).

66. G. Pula, M. Krause, Role of Ena/VASP proteins in homeostasis and disease. *Handb. Exp. Pharmacol.* **186**, 39–65 (2008), 10.1007/978-3-540-72843-6_3.

67. F. D. Smith, J. D. Scott, Scaffolding proteins: Not such innocent bystanders. *Curr. Biol.* **23**, R515–R517 (2013).

68. B. T. Goult, M. von Essen, V. P. Hytonen, The mechanical cell - the role of force dependencies in synchronising protein interaction networks. *J. Cell Sci.* **135**, jcs259769 (2022).

69. Y. Wang, J. Yan, B. T. Goult, Force-dependent binding constants. *Biochemistry* **58**, 4696–4709 (2019).

70. P. J. Bucko, J. D. Scott, Drugs that regulate local cell signaling: AKAP targeting as a therapeutic option. *Annu. Rev. Pharmacol. Toxicol.* **61**, 361–379 (2021).

71. J. Troger, M. C. Moutty, P. Skroblin, E. Klussmann, A-kinase anchoring proteins as potential drug targets. *Br. J. Pharmacol.* **166**, 420–433 (2012).

72. A. Ruppelt *et al.*, Inhibition of T cell activation by cyclic adenosine 5′-monophosphate requires lipid raft targeting of protein kinase A type I by the A-kinase anchoring protein ezrin. *J. Immunol.* **179**, 5159–5168 (2007).

73. D. Diviani, L. K. Langeberg, S. J. Doxsey, J. D. Scott, Pericentrin anchors protein kinase A at the centrosome through a newly identified RII-binding domain. *Curr. Biol.* **10**, 417–420 (2000).

74. S. Seetharaman *et al.*, Microtubules tune mechanosensitive cell responses. *Nat. Mater.* **21**, 366–377 (2022).

75. C. Ciobanasu, B. Faivre, C. Le Clainche, Actomyosin-dependent formation of the mechanosensitive talin-vinculin complex reinforces actin anchoring. *Nat. Commun.* **5**, 3095 (2014).

76. R. B. Khan, B. T. Goult, Adhesions assemble!-autoinhibition as a major regulatory mechanism of integrin-mediated adhesion. *Front. Mol. Biosci.* **6**, 144 (2019).

77. P. Atherton *et al.*, Vinculin controls talin engagement with the actomyosin machinery. *Nat. Commun.* **6**, 10038 (2015).

78. B. Klapholz, N. H. Brown, Talin–the master of integrin adhesions. *J. Cell Sci.* **130**, 2435–2446 (2017).

79. J. Robertson *et al.*, Defining the phospho-adhesome through the phosphoproteomic analysis of integrin signalling. *Nat. Commun.* **6**, 6265 (2015).

80. K. Isobe *et al.*, Systems-level identification of PKA-dependent signaling in epithelial cells. *Proc. Natl. Acad. Sci. U.S.A.* **114**, E8875–E8884 (2017).

81. D. M. Embogama, M. K. Pflum, K-BILDS: A kinase substrate discovery tool. *Chembiochem* **18**, 136–141 (2017).

82. X. Gao, C. Jin, J. Ren, X. Yao, Y. Xue, Proteome-wide prediction of PKA phosphorylation sites in eukaryotic kingdom. *Genomics* **92**, 457–463 (2008).

83. M. L. Henrich *et al.*, Universal quantitative kinase assay based on diagonal SCX chromatography and stable isotope dimethyl labeling provides high-definition kinase consensus motifs for PKA and human Mps1. *J. Proteome Res.* **12**, 2214–2224 (2013).

84. H. Imamura, N. Sugiyama, M. Wakabayashi, Y. Ishihama, Large-scale identification of phosphorylation sites for profiling protein kinase selectivity. *J. Proteome Res.* **13**, 3410–3419 (2014).

85. H. Imamura *et al.*, Identifications of putative PKA substrates with quantitative phosphoproteomics and primary-sequence-based scoring. *J. Proteome Res.* **16**, 1825–1830 (2017).

86. P. Giansanti, M. P. Stokes, J. C. Silva, A. Scholten, A. J. Heck, Interrogating cAMP-dependent kinase signaling in Jurkat T cells via a protein kinase A targeted immune-precipitation phosphoproteomics approach. *Mol. Cell. Proteomics: MCP* **12**, 3350–3359 (2013).

87. G. P. Coló, E. M. Lafuente, J. Teixidó, The MRL proteins: Adapting cell adhesion, migration and growth. *Eur. J. Cell Biol.* **91**, 861–868 (2012).

88. H. Döppler, P. Storz, Regulation of VASP by phosphorylation: Consequences for cell migration. *Cell Adh. Migr.* **7**, 482–486 (2013).

89. A. Kumar *et al.*, Local tension on talin in focal adhesions correlates with F-actin alignment at the nanometer scale. *Biophys. J.* **115**, 1569–1579 (2018).

90. S. F. H. Barnett, B. T. Goult, The MeshCODE to scale-visualising synaptic binary information. *Front. Cell Neurosci.* **16**, 1014629 (2022).

91. L. E. Young, H. N. Higgs, Focal adhesions undergo longitudinal splitting into fixed-width units. *Curr. Biol.* **28**, 2033–2045.e2035 (2018).

92. A. W. M. Haining *et al.*, Mechanotransduction in talin through the interaction of the R8 domain with DLC1. *PLoS Biol.* **16**, e2005599 (2018).

93. G. Li *et al.*, Full activity of the deleted in liver cancer 1 (DLC1) tumor suppressor depends on an LD-like motif that binds talin and focal adhesion kinase (FAK). *Proc. Natl. Acad. Sci. U.S.A.* **108**, 17129–17134 (2011).

94. S. Kaushik, A. Ravi, F. M. Hameed, B. C. Low, Concerted modulation of paxillin dynamics at focal adhesions by Deleted in Liver Cancer-1 and focal adhesion kinase during early cell spreading. *Cytoskeleton (Hoboken)* **71**, 677–694 (2014).

95. F. C. Ko *et al.*, PKA-induced dimerization of the RhoGAP DLC1 promotes its inhibition of tumorigenesis and metastasis. *Nat. Commun.* **4**, 1618 (2013).

96. X. Cao, C. Voss, B. Zhao, T. Kaneko, S. S. Li, Differential regulation of the activity of deleted in liver cancer 1 (DLC1) by tensins controls cell migration and transformation. *Proc. Natl. Acad. Sci. U.S.A.* **109**, 1455–1460 (2012).

97. Y. C. Liao, S. H. Lo, Tensins–emerging insights into their domain functions, biological roles and disease relevance. *J. Cell Sci.* **134** (2021).

98. P. Atherton *et al.*, Tensin3 interaction with talin drives the formation of fibronectin-associated fibrillar adhesions. *J. Cell Biol.* **221**, e202107022 (2022).

99. A.K. Howe, Kang_PNAS2024. Howelabuvm. https://github.com/howelabuvm/Kang_PNAS2024. Deposited 30 January 2024.

100. M. C. Jones *et al.*, Isolation of integrin-based adhesion complexes. *Curr. Protoc. Cell Biol.* **66**, 9.8.1–9.8.15 (2015).

101. S. P. Skinner *et al.*, Structure calculation, refinement and validation using CcpNmr analysis. *Acta Crystallogr. D Biol. Crystallogr.* **71**, 154–161 (2015).